Improvement of the Surface Quality of Foam Injection Molded Products from a Material Property Perspective

Weiyuan Lin, Yoshiki Hamamoto, Yuta Hikima, Masahiro Ohshima

Department of Chemical Engineering, Kyoto University, Kyoto 615-8510, Japan

Keywords: foams, injection molding, surface, crystallization, viscosity, polyolefins

ABSTRACT: Microcellular injection molding is an attractive method. However, their surface imperfections have been a major problem hindering wide industrial applications. Several methods have been proposed to improve the surface appearance of foams. In this study, we proposed a method to improve the surface appearance of polypropylene foams from the material property perspective, especially with regard to crystallization and viscosity. The basic idea of the surface improvement is to reduce the size of bubbles generated at the flow front, delay the solidification behavior of the polymer at the mold interface, squeeze the bubbles existing at the mold-polymer interface, and redissolve the bubbles into the polymer by holding pressure. Blending a low modulus polypropylene (PP) delays the crystallization of the polymers at the skin layer and solidification, taking enough time to squeeze the bubbles smaller. A sorbitol-based gelling agent, (bis-O-(4 methylphenyl) methylene)-D-Glucitol), was used to increase the viscosity at a low strain rate to reduce the size of the bubbles generated at the flow front during the filling stage. The foam injection molding experiments demonstrated that the proposed method effectively improved the surface appearance of the foams. In particular, the surface appearance of the foams became almost equivalent to that of solid samples using low-modulus polypropylene.

INTRODUCTION

Microcellular plastic foaming with environmentally benign foaming agents is a technique of growing interest that contributes to sustainable development [1-4]. Compared with standard polymer foams, microcellular foams of cell sizes less than 100 μm and cell densities higher than 10^8 cells/cm^3 show a higher strength-to-weight ratio, better dimensional stability, and lower

deterioration of mechanical strength. These features provide microcellular foams with various applications including packaging materials, sports equipment, automobile parts, and thermal insulators [5-6]. Since microcellular plastic foams were invented, numerous studies have been conducted on processes and materials. Microcellular foams were produced using batch, extrusion, bead foaming, and foam injection molding (FIM) processes [1]. Among these processes, FIM was considered cost-effective for producing microcellular plastic foams because of its shorter molding cycles. Furthermore, combining microcellular foam injection molding with a core-back or precise mold opening operation could produce higher expansion foams with fine cellular structures.

Despite these advantages, the low surface quality of FIM microcellular foam is a significant problem that limits its industrial applications, especially in the usage of exterior parts. Swirl marks and silver streaks are two common defects that seriously deteriorate the surface appearance of foams. The swirl marks and silver streaks were gas flow marks caused by bubbles trapped on the mold surface when the injected molten polymer was solidified. These were caused mainly by a mechanism in which bubbles were nucleated at the melt flow front in the filling stage, stretched, broken, pushed to the mold side by the fountain flow behavior, and tapped [7-9]. The large broken cells on the surface caused the swirl marks, while the smaller oriented cells formed silver streaks [8].

Several studies have been conducted to reduce and eliminate these surface imperfections. Lee et al. [10] aimed to improve the surface quality by reducing the bubble nucleation rate. They decreased the degree of supersaturation of the physical blowing agent (PBA) in the injected polymer to lower the bubble nucleation rate at the melt flow front. They succeeded in reducing the swirl marks; however, their scheme contradicted the production of fine foams with a high expansion ratio, which usually requires higher gas content and a higher degree of supersaturation of the PBA.

A typical scheme for improving the surface quality of foams is to control the mold temperature using mold temperature control units with several thermal heating devices or insulators. The scheme was initially developed for erasing weld lines. The rapid heat and cooling mold technique (RHCM) and thermal cycling molding (RTCM) are two representative techniques of the scheme [11-17]. In these technologies, the mold cavity surface is heated rapidly, and during the filling stage, the mold wall temperature is kept high enough for bubbles at the mold surface to

be eliminated [13-15]. Some thermal insulators might be inserted into the mold to keep the interface temperature between the mold and the injected molten polymer high [16, 17]. The mold temperature control methods are effective; however, the cost of the mold is increased, and the production cycle time is also increased.

The gas counterpressure (GCP) process is another approach that can suppress bubble nucleation at the flow front during the filling stage [18-20]. Before injecting the polymer, high-pressure gas is introduced into the mold cavity to suppress bubble nucleation at the flow front. Then, the pressure is released through a vent hole of the mold before completely filling out the cavity with the polymer. Related to the technique using gas pressure, Hou and coworkers developed a method of combining gas-assisted microcellular injection molding (GAMIM) [21]. In operation, pressurized gas is injected into a foaming core polymer through the gas inlets to ensure the completion of the filling stage. Then, the high pressure is held for a certain period to compress the injected polymer to the mold surface and squeeze or erase the bubbles on the surface.

Other methods of improving the surface quality are the in-Mold decoration process (IMD) and co-injection or sandwich injection molding, where a solid skin material (metallic or polymeric parts) is introduced before a foaming core polymer is injected [22,23]. By building a sandwiched structure (solid skin-foam core-solid skin), the imperfection of the foam parts is concealed with the introduced skin materials. Guo et al. reported an interesting experimental result using a mold wall decollated with PET film [24]. The film achieved an asymmetrical temperature distribution. Then, bubbles traveled to the PET side due to higher temperature and were flattened by significant shear flow.

From the viewpoint of polymer properties, some methods have been proposed. Lee et al. improved the surface quality of LDPE foams by using a low-molecular-weight polymer as a slip agent [25]. Wang et al. used a nanofiller to enhance the melt strength and the surface quality of PP nanocellular foams prepared by foam injection molding technology [26]. The bubbles can be visually ignored because of their small size [27]. From the early stage of microcellular foam development, it has been believed that higher melt strength or strain hardening behavior is a beneficial polymer property for forming tiny bubbles and preventing bubble breakup during the filling stage [28-29].

As mentioned above, there are many promising methods for improving the surface quality of foam. Two common key concepts exist in those methods, excluding the IMD. One is to reduce the number and size of the bubbles nucleated at the melt front during the filling stage. The other is to squeeze and erase the bubbles by giving some stress before the polymer is solidified. In this study, keeping these two key concepts in mind, we proposed a method of improving the surface quality of polypropylene (PP) microcellular foams from the polymer property aspect. PP is a commercial semicrystalline thermoplastic polymer, and PP microcellular foams have been developed for several automobile parts because of their light weight, low cost, and easy recycling [30,31]. Low-modulus polypropylene (LMPP) and a sorbitol-based gelling agent (bis-O-(4 methyl phenyl) methylene)-D-Glucitol) were used to improve the surface quality of the PP microcellular foams. The gelling agent (MD) prevents bubbles from growing and reduces bubble size. LMPP slows the PP crystallization rate, lowers the viscosity of the polymer at the interface, and delays the crystallization at the skin, resulting in producing enough time to squeeze the bubbles on the surface. Using this additive and blending with a low-crystalline polymer, we conducted several microcellular foam injection molding experiments with the core-back operation by changing the LMPP blend ratios.

EXPERIMENTAL

Materials

Homopolypropylene (HPP, J105G, Prime Polymer Co., Ltd., Japan) with a weight-average molecular weight (M_w) of 260 000 g/mol and melt flow rate (MFR) of 9.0 g/10 min (at 230 ℃) was used as the base resin. Low modulus polyolefin (LMPP: L-MODU S901, Idemitsu Kosan Co., Ltd., Japan) with 130000g/mol M_w and a 50 g/10 min melt flow rate (at 230 ℃) was used as a blend polymer to control the crystallization rate and crystallization temperature. The blend ratios tested in this study are summarized in Table 1 with the abbreviations of the sample name. The sorbitol-based gelling agent (bis-O-(4 methylphenyl) methylene-D-Glucitol: MD, New Japan Chemical Co., Ltd., Japan) was used to control the viscosity at a low strain rate range. A master batch of PP with 3%MD additive was compounded and provided by the same company. When MD was used, the master batch was mixed with the HPP/LMPP blends at the hopper to be 0.3 or 0.5 wt.% content. Since a higher content of MD induces agglomeration of the additive and results

in less efficacy, MD was reduced to the most effective content [32]. Nitrogen (N_2, Izumi Sanyo, Japan) with 99.9% purity was used as a physical blowing agent (PBA).

TABLE 1. Compositions of investigated polymers

Blend	Blend ratio (wt %)
HPP	100/0
HPP/20%LMPP	80/20
HPP/30%LMPP	70/30
HPP/40%LMPP	60/40
HPP/60%LMPP	40/60
HPP/0.3%MD	99.7/0/0.3
HPP/30%LMPP/0.3%MD	69.7/30/0.3

Foaming Experiments

Foam injection molding experiments were conducted using a 35-ton clamping force MuCell machine (J35EL III-F, Japan Steel Work, Japan) with a gas delivery unit (SCF device SII TRJ-10-A-MPD, Trexel Inc., USA). A cylindrical screw 20 mm in diameter with an L/D ratio of 40:1 and a mold with a rectangular-shaped cavity (70 mm × 50 mm × 1 mm) were used for injection molding experiments. N_2 was pressurized to 24 MPa by the gas delivery system and injected into the molten polymer in the middle of the barrel of the injection molding machine through an injector valve. A single-phase solution of molten polymer and 0.11 wt.% N_2 was injected into the mold cavity. The N_2 concentration was controlled by manipulating the injector valve opening time. The details of the mold geometry and operation of FIM are described in our previous papers [32, 33]. The nozzle zone and metering zones of the injection molding machine were set at 200 °C. The mold temperature was maintained at 40 °C. Two infrared temperature sensors and two pressure sensors were independently deployed in the mold cavity to measure the polymer temperatures and pressures at different locations in the cavity: one location was close to the inlet, and the other was at the flow end, as shown in Figure 1. By averaging the temperatures and pressures at two points of three injection cycles, the temperature and the pressure profiles during a cycle of injection molding were calculated and plotted against the processing time, as shown in Figure S1 of the Supporting Information. The infrared temperature sensors can measure the polymer temperature at approximately 0.4 mm inside from the mold-polymer interface in the thickness direction. The

cooling rate of the polymer in the holding process was estimated from the recorded temperature profiles to be -** °C/s on average.

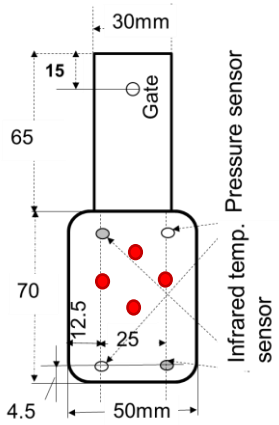

FIGURE 1. Geometry of injection-molded sample, sensor locations, and roughness measuring points.

FIM with core-back (precise mold opening) operation was applied to produce foams. The difference between core-back and conventional FIM lies in an additional mold-opening operation. In the core-back FIM process, a part of the mold is quickly opened to expand cavity volume. This mold opening operation initiates bubble nucleation and growth by the rapid pressure drop and produces a cellular structure. In the experiments, the mold part was opened at a rate of 20 mm/s. The expansion ratio of foams was set to five by setting the core-back (mold opening) distance to 4 mm from a 1-mm initial cavity thickness (total 5 mm in foam thickness). The processing parameters are summarized in Table 2.

TABLE 2. Processing parameters of foam injection molding with core-back operation.

Parameters	Values
Polymer temperature [°C]	200
Mold temperature [°C]	40
Injection speed [mm/s]	80
Screw back pressure [MPa]	15
Packing (holding) pressure [MPa]	40
Cooling time [s]	30
Core-back distance [mm]	4
Core-back speed [mm/s]	20

Metering distance [mm]	35
N_2 content [%]	0.11

Rheological Characterization

Strain-controlled dynamic frequency sweep and temperature sweep rheological measurements were conducted using a rheometer (ARES, TA Instruments, Inc., New Castle, DE, USA) with a 25-mm parallel-plate device. Before the measurement, specimens 25 mm in diameter and 2 mm in thickness were prepared using a hot compressing machine at a temperature of 200 ℃ and compression pressure of 20 MPa. Frequency sweep tests for HPP and HPP/LMPP blends were carried out by changing the shear rate frequency from 100 to 0.1 rad/s with 1% strain at a temperature of 200 ℃. This was kept at 200 ℃ for 3 min to erase the thermal history. To further clarify the effect of MD in the frequency sweep test, the experimental temperature was also set at 170 ℃ for HPP, HPP/30%LMPP, HPP/0.3%MD, and HPP/30%LMPP/0.3%MD. Prior to the experiment, the temperature was increased to 230 ℃ and kept for 3 min to erase the effect of PP crystallization and completely dissolve MD into PP. The temperature sweep measurements were conducted at 100–200 ℃ with a 1% strain amplitude and 0.63 rad/s. The damping rate was set at 5 ℃/min.

Measurement of Thermal Properties

Isothermal and nonisothermal measurements were conducted using a Flash DSC1 (Mettler-Toledo, LLC, USA) under N_2 purging. For isothermal measurement, the temperature was first heated to 230 ℃, held for 1 s, reduced at a cooling rate of 4000 ℃/s, and held at a designated isothermal crystallization temperature. The heat generation or crystallization enthalpy was measured for the isothermal temperature designated in the range of 0 to 110 ℃. The isothermal crystallization rate and the half crystallization time were estimated by fitting Eqs. (1) and (2) [34] to the DSC data.

$$\log\{-\ln[1 - X(t)]\} = \log k + n \log t \qquad (1)$$

$$t_{1/2} = \left(\frac{\ln 2}{k}\right)^{1/n} \qquad (2)$$

where $X(t)$ represents the relative crystallinity, k is the crystallization rate, and t is the time. n is the Avrami index, and $t_{1/2}$ is the half crystallization time.

Since the cooling rate of the injected polymer in the mold cavity was estimated to be -35 ℃/s on average, as illustrated in Figure S1, nonisothermal measurement was conducted by cooling the polymer samples at -35 ℃/s after heating to 230 ℃ at 1000 ℃/s. Then, the effect of LMPP on the crystallization temperature was observed from the heating curve.

Surface Roughness Analysis

The surface roughness of the foams was quantitatively measured using a laser microscope (LEXT OLS4100, Olympus, Japan). The cutoff values of the high-pass filter λ_c and low-pass filter λ_s were set to 2500 and 0 μm, respectively. The cutoff values of the two filters were tuned to reduce the influence of undulation and observe the silver stream or bubble footprint clearly. The magnification of the microscope was 5x. Four points on every three injection molded samples were selected for each foam injection molding condition to measure the roughness. The four points measuring the surface roughness are indicated in Figure 1.

The surface roughness was calculated with the arithmetical mean height (*Sa*) value, Eq. (3): A lower *Sa* indicates fewer defects and a smoother surface area.

$$Sa = \frac{1}{A}\iint_A |Z(x,y)|\, dxdy \qquad (3)$$

where *A* is the measuring area, and *Z* (*x*, *y*) indicates the height of the surface at locations *x* and *y*.

In addition to the *Sa* value, 2D and 3D images of foam surfaces were taken by laser microscopy to clearly verify the effect of LMPP and MD on surface quality. The cutoff values of high-pass and low-pass filters were set to 2500 and 30 μm for 3D laser images to reduce the influence of noise.

The surface visual appearance was observed by employing a digital camera. Carbon black was added to all polymers to clearly observe the silver streaks or the swirl mark on the surface of the injection molded samples.

Observation of Cell Morphology

A small sliced specimen was cut from the foam injection-molded product after cryogenically solidified in liquid nitrogen for cell morphology observation with a scanning electron microscope (SEM: Tiny-SEM, Technex, Japan). The observation was made in both perpendicular and parallel directions to the core-back direction, i.e., the thickness direction of the foam, as prepared in previous work [32].

RESULTS AND DISCUSSION

Rheological Properties

Figure 2 shows the temperature-sweep measurements of the complex viscosities of four materials (HPP, HPP/20%LMPP, HPP/40%LMPP, and HPP/60%LMPP) measured at a cooling rate of -5 ℃/min. The viscosities of these four materials increased as the temperature decreased. Blending LMPP reduced the viscosity to a lower value than that of the neat HPP. As shown in Figure 2, all materials showed a drastic change in viscosity in the range of 120-130 ℃. This change indicates the occurrence of crystallization, and the corresponding turning point temperature can be regarded as the crystallization temperature at a cooling rate of -5 ℃/min. The crystallization onset temperature of neat HPP was 125.86 ℃, while those of PP/20%, 40%, and 60% LMPP were 124.12 ℃, 121.35 ℃, and 119.19 ℃, respectively. The crystallization onset temperature shifted to a lower temperature with increased LMPP content. The decreased crystallization temperature indicates that LMPP acts as a crystallization retarding agent in the blend. Figure S2 shows the viscosities of HPP and HPP/LMPP blends as a function of frequency. As the LMPP content increased, the viscosity decreased over the entire frequency range. It is also noticeable that the viscosities of all materials decreased in the high-frequency region.

The influence of MD on the viscosity of HPP was investigated by temperature and frequency sweep tests. As reported previously [32, 35, 36], adding MD to PP increases the viscosity and the melt strength. Because the formation of the nanofibril network of MD occurs as a phase separation phenomenon of MD from the molten polymer [32], the complex viscosity increased at temperatures below 170 ℃, as shown in Figure 3. This viscosity increase widens the foaming temperature window for suppressing bubble growth and keeping the bubble size on the micrometer scale [35-36]. Figure S3 shows the frequency-sweep complex viscosity of HPP and

HPP/LMPP with 0.3% MD addition. The temperatures of measurement were 200 ℃ and 170 ℃. Figure S3a shows the complex viscosities of these materials at 200 ℃. It is clear that HPP/0.3%MD had the highest viscosity among these materials across the entire frequency range. Moreover, viscosity decreased with LMPP addition. Figure S3b shows the complex viscosities of these materials at 170 ℃. The viscosities of HPP/0.3%MD and HPP/30%LMPP/0.3%MD were higher than those of HPP and the HPP/LMPP blend, respectively, due to reinforcement of MD. The presence of in situ formation of the MD nanofibril network in the molten polymer [32] increases the viscosity of HPP and HPP/LMPP in the low-frequency (strain rate) range. These changes in the rheology of PP possibly provide the benefit of reducing the bubble size not only for bubbles generated in the foam core part but also those generated at the flow front of the injected polymer.

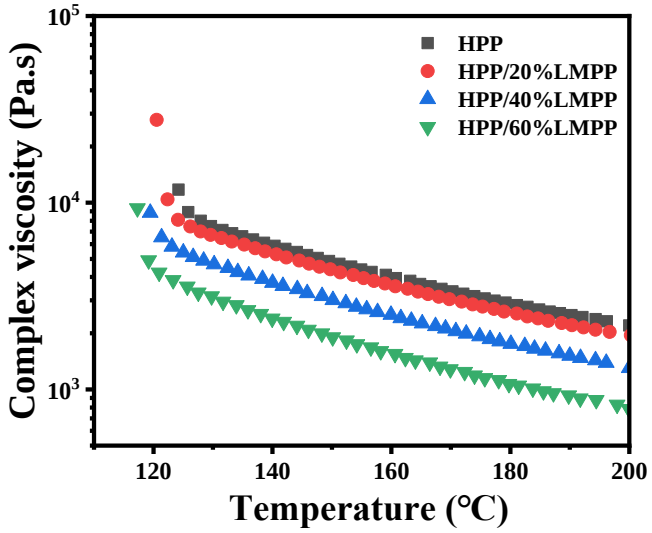

FIGURE 2. Complex viscosity of neat HPP and HPP/LMPP blends with 20, 40, and 60 wt.% LMPP content as a function of temperature.

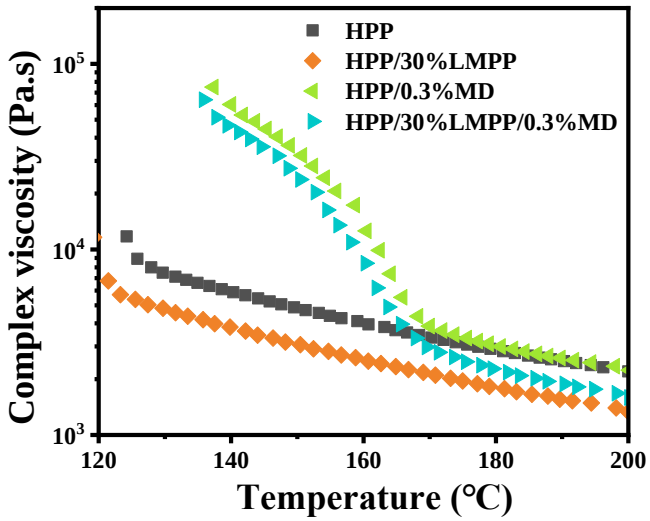

FIGURE 3. Complex viscosity of HPP, HPP/30%LMPP, HPP/0.3%MD, and HPP/30%LMPP/ 0.3%MD against temperature.

Crystallization Kinetics at High Cooling Rate

Flash DSC measurements were conducted to clarify the crystallization retarding effect of the LMPP for both isothermal crystallization and faster cooling (nonisothermal) conditions. Figure 4 shows the results of the crystallization rate k and half crystallization time $t_{1/2}$ of HPP and HPP/LMPP blends for isothermal crystallization conditions. In Figure 4a, the crystallization rate of HPP was highest at all temperatures. With an increase in LMPP content, the crystallization rate was reduced. The crystallization rate of HPP/60%LMPP could be lower than 1 s^{-1} at 40 °C, which corresponds to the molding temperature. As the LMPP content increased, the half crystallization time became considerably longer, as shown in Figure 4b. Both results in Figure 4 indicate that LMPP delays the crystallization of HPP.

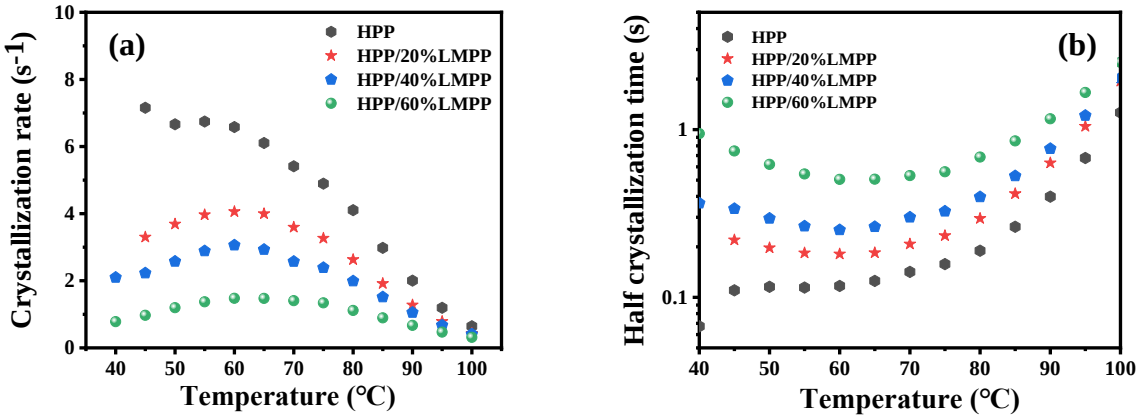

FIGURE 4. Crystallization rate and half crystallization time of HPP and HPP/LMPP blends.

Figure 5 shows the heat generation curves of the nonisothermal condition at a cooling rate of -35 ℃/s for HPP/LMPP blends. The temperature at which the curves peaked was regarded as the crystallization temperature. The crystallization temperature results are listed in Table 3 for each sample. The crystallization temperature decreases as the LMPP content increases. No crystallization peak was observed when the LMPP was increased to 60%. These results indicate that LMPP delays HPP crystallization even for fast-cooling conditions such as the mold cavity cooling rate.

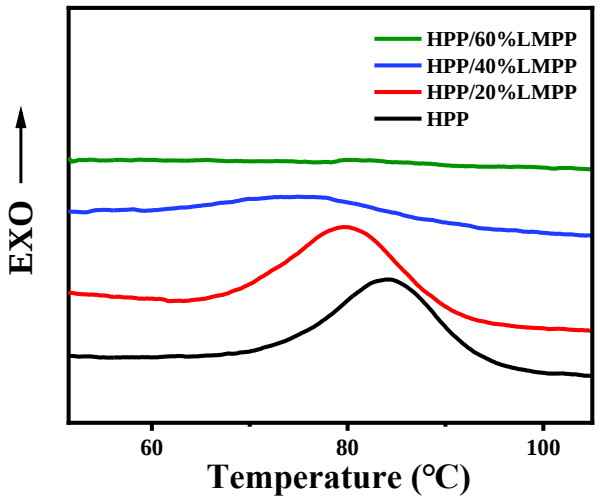

FIGURE 5. Cooling curves of HPP and HPP/LMPP blends measured at a cooling rate of -35 ℃/s.

TABLE 3. Crystallization peaks of HPP and HPP/LMPP blends at a cooling rate of -35 ℃/s.

Parameters	HPP	HPP/20% LMPP	HPP/40% LMPP	HPP/60% LMPP
Peak Temperature [℃]	85.59	81.49	76.89	-

Surface Roughness Evaluation

Figure 6 shows the *Sa* of foam injection-molded parts prepared from HPP and HPP/LMPP with different blend ratios. The HPP solid (nonfoamed) sample had the lowest *Sa* at ca. 2.02 μm. When polymers were foamed with N_2, *Sa* of HPP foam samples increased to ca. 9.79 μm, indicating an increase in surface roughness. The *Sa* of the foam-injection-molded part decreased with increasing LMPP content. The values of *Sa* for foams of HPP/20%, 30%, 40%, and 60% LMPP were 9.10, 9.02, 6.08 and 4.03 μm, respectively. When LMPP was blended at 60%, the surface of the foams became almost equivalent to that of HPP solid by naked eye and laser microscope images of λ_s=30 μm.

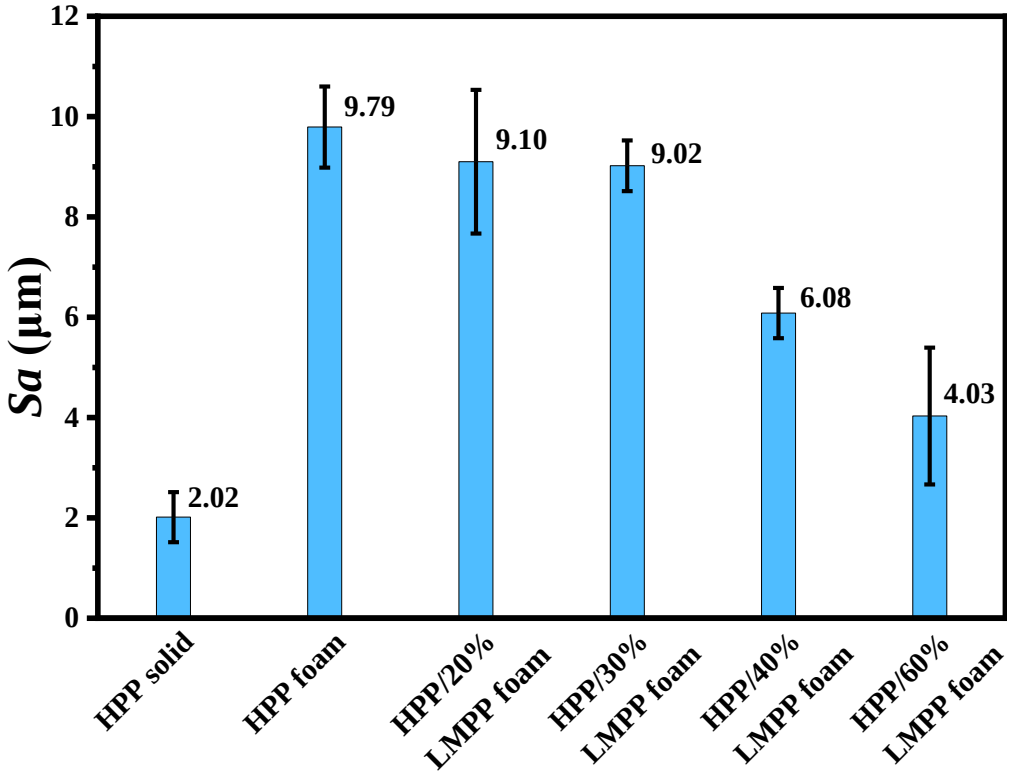

FIGURE 6. Surface roughness (*Sa*) of HPP solid, HPP foam and HPP/LMPP foams with different blend ratios.

In the Supporting Information, Figure S4 shows the *Sa* of the foamed injection molded HPP with two different amounts of MD: 0.3 and 0.5 wt.%. As we expected, adding MD can improve the surface quality. Figure 7 shows the *Sa* values of foam-injection-molded parts prepared from HPP (solid), foamed HPP, HPP/0.3%MD, and HPP/30%LMPP with 0.3%MD. As shown in Figure 7, when MD (0.3%) was used together with 30%LMPP, the surface roughness was lower than that of HPP/40%LMPP (Figure 6) and became closer to that of the HPP solid injection molded parts. This indicates that a synergetic effect of MD and LMPP occurs to improve the surface quality.

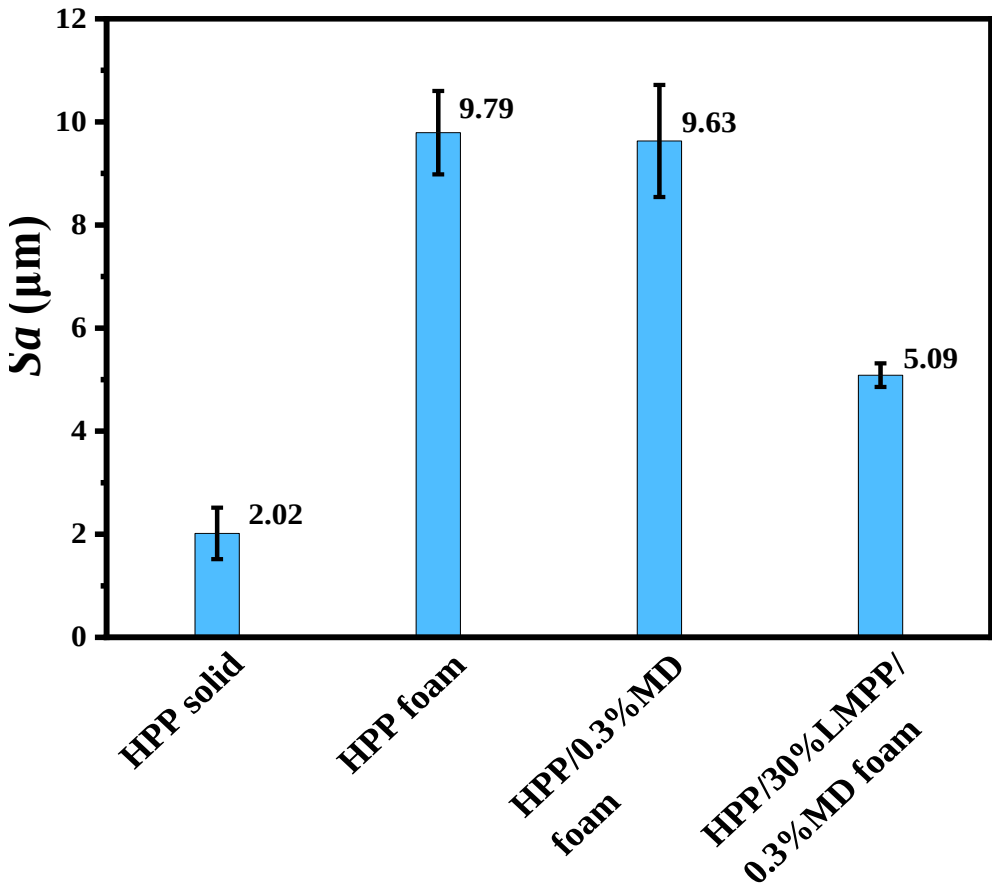

FIGURE 7. Surface roughness (*Sa*) of HPP solid, HPP foam, HPP/0.3%MD foam, and HPP/30%LMPP/0.3%MD foam

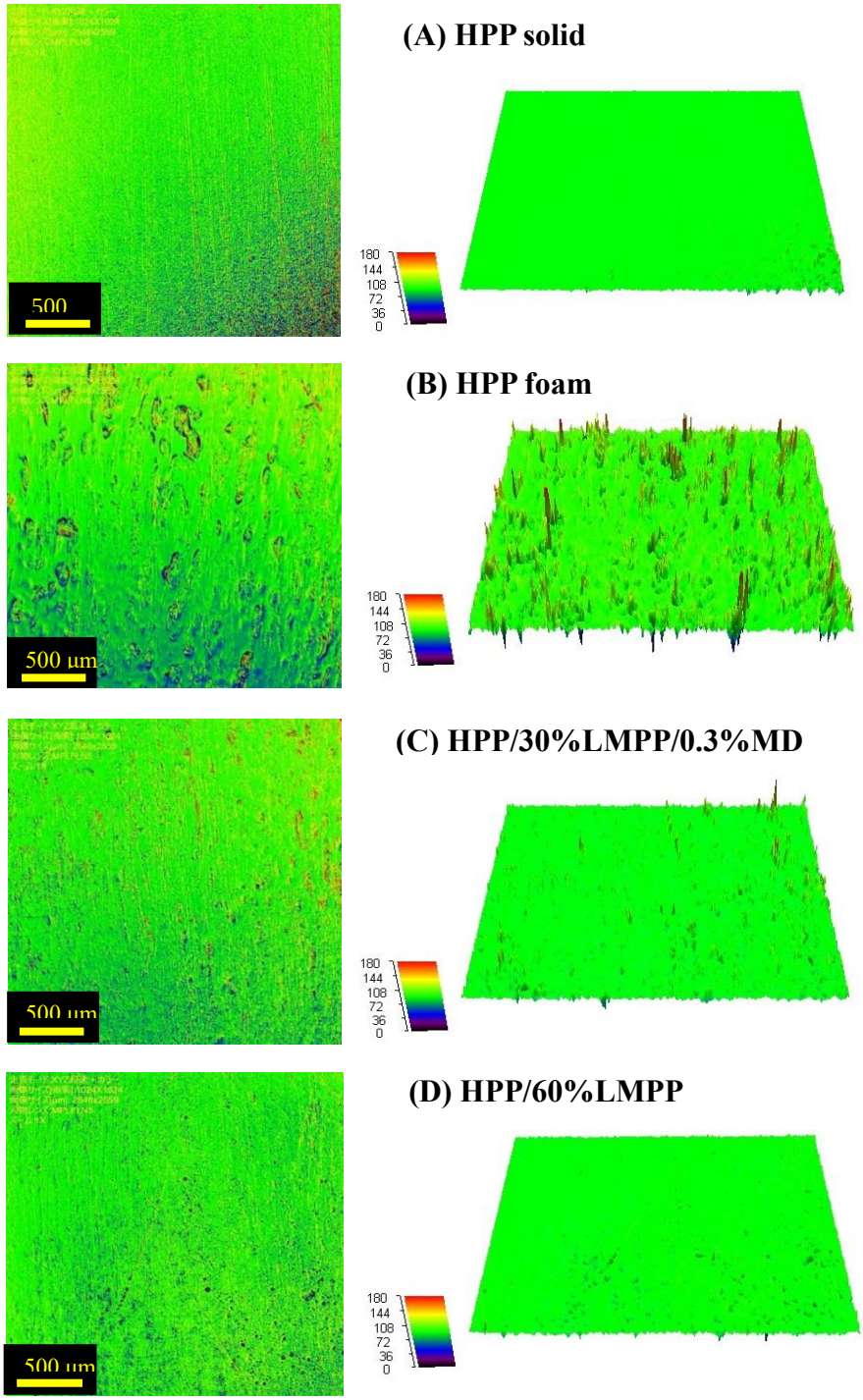

FIGURE 8. Two-dimensional (2D) and Three-dimensional (3D) laser microscope images of injection molded parts: (A) HPP solid, (B) HPP foam, (C) HPP/30%LMPP/0.3%MD foam, and (D) HPP/60%LMPP foam. For 2D (λ_c = 2500 µm and λ_s = 0 µm) and 3D (λ_c = 2500 µm and λ_s = 30 µm).

Figure 8 shows the 2D and 3D images of the surfaces of injection-molded solid HPP, HPP foam, HPP/30%LMPP/0.3%MD foam, and HPP/60%LMPP foam. The observation areas of both the 2D and 3D images were fixed at 2548×2559 μm^2. When foam injection molding was conducted, serrations or ripples were observed in the 2D and 3D laser microscope images of the HPP foam, corresponding to the footprints of the bubbles on the surface. For HPP/60%LMPP, there are few serrations and ripples, and the image is very close to that of HPP solid. When compare the image of HPP/30%LMPP/0.3%MD foam with HPP/30%LMPP shown in Figure S6b of the Supporting Information, the efficacy of MD on the surface roughness can be seen.

Figure 9 shows digital camera images of the injection-molded parts. A carbon black (CB) color batch pellet made of 60 wt.% polyethylene (MFR=15) and 40 wt.% CB was added to each investigated polymer to observe the silver streak and bubbles on the foam surface easily by the naked eye. The upper right figure is a magnified image of each sample. HPP/30%LMPP/0.3%MD foam shows low surface roughness, but footprints of silver streaks remain. These surface imperfections vanished when the HPP was increased to 60 wt.%. The surface quality of the foam was equivalent to that of HPP solid.

The surface quality improvement can be correlated to the crystallization-delaying effect of LMPP and the viscosity effect of MD. The trapped bubbles are known to cause surface roughness during the solidification of foam skin. With the addition of MD, the size of the bubbles generated at the flow front became small and easily squeezed in a short time by the holding pressure. Furthermore, blending LMPP with HPP delays the crystallization of HPP and provides a time to squeeze or erase the bubbles and silver streaks by the holding pressure before the solidification of the injected polymer is completed. The 60%LMPP blend prevents the injected polymer from crystallizing at a fast cooling rate; the surface of the HPP/60%LMPP blend foam becomes equivalent to that of the HPP solid.

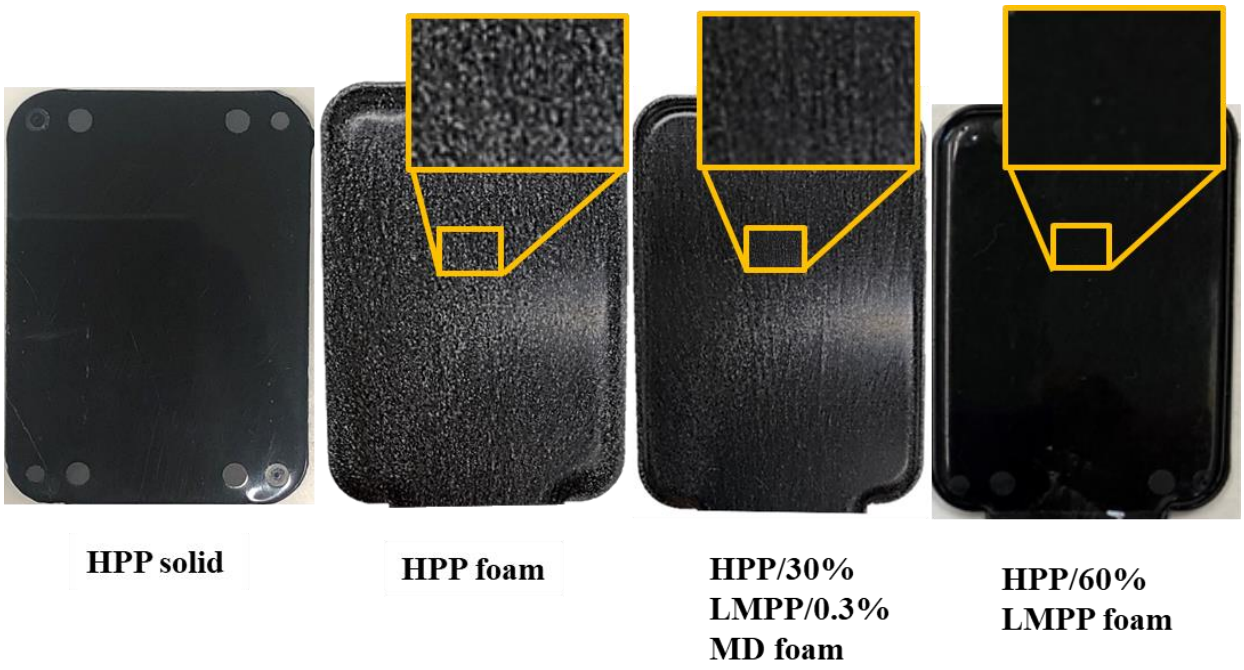

FIGURE 9. Digital camera images of nonfoamed HPP, HPP foam, HPP/30%LMPP/0.3%MD foam, and HPP/60%LMPP foam.

Effect of LMPP and MD on Cell morphology

Figures 10 and S9 illustrate the SEM images of the cell morphology of the five-fold expanded foams. Each figure's left-side image was a cross-sectional area near a skin layer of the foam, taken from a view parallel to the core-back direction, i.e., foam thickness direction. The right-side image was a cross-sectional area of the foam core, taken from a view perpendicular to the core-back direction. The dotted circle indicates the presence of elongated bubbles on the surface. As seen in Figure 10, elongated bubbles on the surface of the HPP/60%LMPP and HPP/30%LMPP/0.3%MD are rarely seen while they could be observed on the surface of HPP foam.

All polymers could be foamed to be five-fold by manipulating the foaming temperature. The cell morphology was dependent on the core-back time, i.e., foaming temperature. The foaming temperature was the temperature at the point where the core-back operation was conducted, as shown in Figure S1. The longer the core-back time is, the lower the foaming temperature becomes.

With the increased LMPP content, the cell size became larger, as observed in SEM cell morphology images of HPP (Figure 10(a)), HPP/20%LMPP (Figure S9a), and HPP/30%LMPP (Figure S9b) prepared at the foaming temperature around 100 ^{o}C. When LMPP was increased by over 60%, the cell size became too large unless the foaming temperature was lowered. By prolonging the core-back time and decreasing the foaming temperature from 100 ^{o}C to 80 ^{o}C, the five-fold expansion foams could be prepared from HPP/60%LMPP with smaller cell sizes than those of HPP and HPP/20%LMPP foams (Figure S9a), as shown in Figure 10 (c).

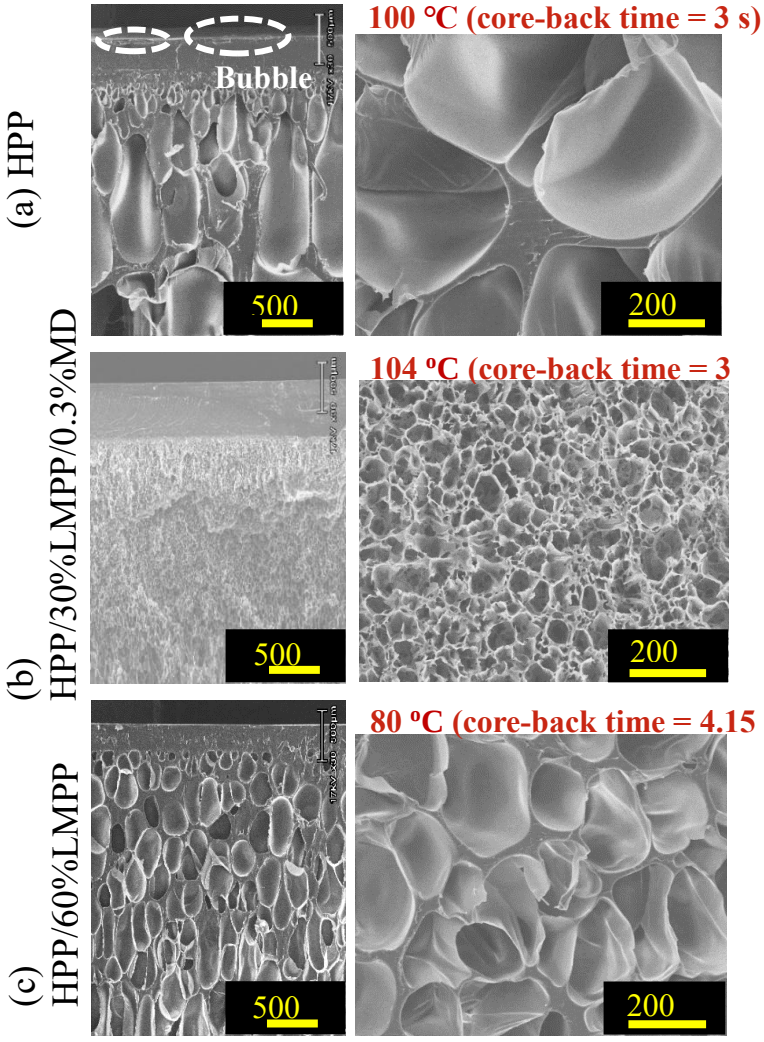

FIGURE 10. SEM images of cell morphology: (a) HPP; (b) HPP/30%LMPP/0.3%MD; (c) HPP/60%LMPP foams at five-fold expansion. Left: a cross-sectional image taken parallel to the core-back direction (thickness direction); Right: a cross-sectional image taken perpendicular to the core-back direction.

Interestingly, with the increase of LMPP, the thickness of the skin layer became thinner owing to viscosity reduction and slow crystallization rate. On the other hand, adding MD made the skin layer thicker when the foams were prepared at the same foaming temperature. However, MD decreased the cell size and improved the cell morphology drastically even when the foams were prepared at a higher temperature. This is because MD reduces the crystal nuclei's size and provides more bubble nucleation sites to the polymer when foaming [32,36].

CONCLUSION

Adding crystal nucleating agent, MD, increases the viscosity with a gelling effect and can reduce the size of bubbles generated at the flow front of injected polymers. Blending a low-modulus polypropylene delays or prevents the crystallization of the injected polymer at the mold interface. The retardation effect on crystallization provides time to squeeze and erase broken bubbles or silver streaks at the skin layers during the holding pressure stage. Blending 60%LMPP with HPP results in silver-streak-free microcellular PP foams. Adding MD and using LMPP can provide synergetic effects on surface quality improvement.

With the increase of LMPP content, mechanical properties such as Yong modulus and Yield stress were lowered, and the polymers' softness was increased, as shown in Figures S7 and S8. However, the foams' mechanical properties depend on the cell morphology. The cell morphology could be controlled by manipulating the core-back time and the degree of expansion ratio.

MD was used to reduce the size of bubbles push to the interface between the mold and polymer. The amount of physical blowing agent (PBA) might be also a key parameter in determining the bubbles' size. When the concentration of the PBA exceeds a certain level where the PBA cannot be entirely dissolved in polymer, or it produces so many bubbles to easily coalesce each other, large size bubbles and swirl mark would appear on the skin layer, which indeed deteriorates the surface appearance. Thus, it can be said that increasing PBA concentration could improve the surface quality as far as the cell size is reduced.

This study demonstrated the feasibility of a surface quality improvement method proposed from the viewpoint of polymer properties, especially with regard to crystallization and viscosity behaviors. Surface imperfections are considered an unavoidable drawback of the microcellular injection molding process. However, this study showed that the problem can be solved by controlling the bubble size and crystallization behavior. The proposed method can be further enhanced by increasing mold temperature or combining the heat and cool method.

ACKNOWLEDGMENT

We sincerely thank Prof. Shuji Matsusaka (Department of Chemical, Kyoto University) for permission to use his laser microscope.

REFERENCES

[1] R. Banerjee, S. S. Ray, *Macromol. Mater*. Eng. 2020, 305, 2000366.

[2] V. Kumar, N. P. Suh, *Polym. Eng. Sci*. 1990, 30, 1323.

[3] J. Jiang, Z. Li, H. Yang, X. Wang, Q. Li, L. S. Turng, *Curr. Opin. Chem. Eng.* 2021, 33, 100694.

[4] Y. Ding, M. H. Hassan, O. Bakker, S. Hinduja, P. Bártolo, *Materials* 2021, 14, 4209.

[5] D. Klempner, K. C. Frisch, *Handbook of Polymeric Foams and Foam Technology*; Hanser Publishers: Munich, 1991.

[6] S. T. Lee, N. S. Ramesh, *Polymeric foams: Mechanical and Materials*; CRC Press: Boca Raton, 2004.

[7] Y. Wang, G. Hu, *Appl. Mech. Mater.* 2011, 66–68, 2010.

[8] G. Hu, B. Hu, *Madridge J. Nanotechnol Nanosci*. 2016, 1, 14.

[9] G. Wang, G. Zhao, J. Wang, L. Zhang, *Polym. Eng. Sci.* 2015, 55, 807.

[10] J. Lee, L. S. Turng, E. Dougherty, P. Gorton, *Polymer* 2011, 52, 1436.

[11] D. E. Pierick, J. R. Anderson, S. W. Cha, L. Chen, J. F. Stevenson, D. E. Laing, US Patent, 6884823, 2005.

[12] Y. Sato, M. Yamaki, M. Nunome, A. Imakawa, M. Takamura, K. Shido, Ono-Sangyo, Mitsui Chemical, JP Patent, 3977565, 2007.

[13] C. L. Xiao, H. X. Huang, X. Yang, *Appl. Therm. Eng*. 2016, 100, 478.

[14] G. Wang, G. Zhao, Y. Guan, *J. Appl. Polym. Sci.* 2013, 128, 1339.

[15] A. Zhang, G. Zhao, Y. Guan, *J. Appl. Polym. Sci*. 2015, 132, 41420.

[16] J. D. Yoon, S. K. Hong, J. H. Kim, *Cell. Polym.* 2004, 23, 39.

[17] J. Lee, L.S. Turng, *Polym. Eng. Sci.* 50 2010, 50, 1281.

[18] A. K. Bledzki, H. Kirschling, G. Steinbichler, P. Egger, *J. Cell. Plast.* 2004, 40, 489.

[19] S. C. Chen, P. S. Hsu, S. S. Hwang, *J. Appl. Polym. Sci*. 2013, 127, 4769.

[20] J. Ren, L. Lin, J, Jiang, Q. Li, S. S. Hwang, *Polymer* 2022, 14, 1078.

[21] J. Hou, G. Zhao, G. Wang, G. Dong, J. Xu, *Mater. Des.* 2017, 127, 115.

[22] L. S. Turng, H. Kharbas, *Int. Polym. Process.* 2004, 19, 77.

[23] E. Suhartono, S. C. Chen, Y. H. Chang, J. A Chang, K. H. Lee, *Int, J. Plast. Technol.* 2017, 21, 239–251.

[24] W. Guo, Q. Yang, H. Mao, Z. Meng, L. Hua, B. He, *Polymers* 2019, 11, 778.

[25] J. Lee, L. S. Turng, J. Peng, E. Dougherty, P. Gorton, *Int. Polym. Process*. 2011, 26, 429.

[26] G. Wang, G. Zhao, L. Zhang, Y. Mu, C. B. Park, *Chem. Eng. J.* 2018, 350, 1.

[27] S. Mendoza-Cedeno, M. S. Kweon, S. Newby, M. Shivokhin, G. Pehlert, P. C. Lee, *Polymers* 2021, 13, 2404.

[28] M. Sugimoto, *J. Soc. Rheol.* 2008, 36, 219.

[29] N. Weingart, D. Raps, M. Lu, L. Endner, V. Altstädt, *Polymers* 2020, 12, 725.

[30] J. Hou, G. Zhao, G. Wang, *J. Mater. Res. Technol.* 2021, 12, 74.

[31] L. Wang, Y. Hikima, S. Ishihara, M. Ohshima, *Ind. Eng. Chem. Res.* 2016, 55, 11970.

[32] R. Miyamoto, S. Yasuhara, H. Shikuma, M. Ohshima, *Polym. Eng. Sci.* 2014, 54, 2075.

[33] L. Wang, Y. Hikima, M. Ohshima, T. Sekiguchi, H. Yano, *RSC Adv.* 2018, 8, 15405.

[34] C. H. Tseng, P. S. Tsai, *Polymers* 2022, 14, 442.

[35] T. Kobayashi and T. Hashimoto, *Bull. Chem. Soc. Jpn.* 2005, 78, 218.

[36] Q. Ren, M. Wu, Z. Weng, L. Wang, W. Zheng, Y. Hikima, M. Ohshima, *J. CO_2 Util.* 2021, 48, 101530.

Figure legends

FIGURE 1. Geometry of injection-molded sample, sensor locations, and roughness measuring points.

FIGURE 2. Complex viscosity of neat HPP and HPP/LMPP blends with 20, 40, and 60 wt.% LMPP content as a function of temperature.

FIGURE 3. Complex viscosity of HPP, HPP/30%LMPP, HPP/0.3%MD, and HPP/30%LMPP/ 0.3%MD against temperature.

FIGURE 4. Crystallization rate and half crystallization time of HPP and HPP/LMPP blends.

FIGURE 5. Cooling curves of HPP and HPP/LMPP blends measured at a cooling rate of -35 ℃/s.

FIGURE 6. Surface roughness (*Sa*) of HPP solid, HPP foam and HPP/LMPP foams with different blend ratios.

FIGURE 7. Surface roughness (*Sa*) of HPP solid, HPP foam, HPP/0.3%MD foam and HPP/30%LMPP/0.3%MD foam.

FIGURE 8. Two-dimensional (2D) and Three-dimensional (3D) laser microscope images of injection molded parts: (A) HPP solid, (B) HPP foam, (C) HPP/30%LMPP/0.3%MD foam, and (D) HPP/60%LMPP foam. For 2D (λ_c = 2500 μm and λ_s = 0 μm) and 3D (λ_c = 2500 μm and λ_s = 30 μm).

FIGURE 9. Digital camera images of nonfoamed HPP, HPP foam, HPP/30%LMPP/0.3%MD foam, and HPP/60%LMPP foam.

FIGURE 10. SEM images of cell morphology: (a) HPP; (b) HPP/30%LMPP/0.3%MD; (c) HPP/60%LMPP foams at five-fold expansion. Left: cross-sectional image taken parallel to the core-back direction (thickness direction); Right: cross-sectional image taken perpendicular to the core-back direction.

TABLE 1. Compositions of investigated polymers.

TABLE 2. Processing parameters of foam injection molding with core-back operation.

TABLE 3. Crystallization peaks of HPP and HPP/LMPP blends at a cooling rate of -35 ℃/s.

FIGURE S1. Pressure and temperature profiles of injection-molded polymer in mold cavity(FIM with core-back operation).

FIGURE S2. Frequency-sweep complex viscosity of HPP and HPP/LMPP blends.

FIGURE S3. Frequency-sweep complex viscosity of HPP, HPP/MD and HPP/LMPP/MD blends at (a) 200 ℃ and (b) 170 ℃.

FIGURE S4. Surface roughness (*Sa*) of HPP solid, HPP foam, HPP/MD (0.3 wt.%) foam and HPP/MD (0.5wt.%) foam..

FIGURE S5. Two-dimensional(2D) and Three-dimensional (3D) laser microscope images of injection-molded parts: (a) HPP/30% LMPP foam, (b) HPP/30% LMPP/0.3%MD foam. (2D: λ_c = 2500 μm and λ_s = 0 μm) and (3D: λ_c = 2500 μm and λ_s = 30 μm).

FIGURE S6. Tensile test data of HPP, HPP/LMPP with different blend ratios, HPP/0.3%MD, HPP/30%LMPP/0.3%MD (non-foamed samples).

FIGURE S7. Young modulus and yield stress of HPP, HPP/LMPP with different blend ratios, HPP/0.3%MD, HPP/30%LMPP/0.3%MD (non-foamed samples).

FIGURE S8. Compression modulus of the HPP foam, HPP/LMPP blends' foams, HPP/LMPP with MD foam.

FIGURE S9. SEM images of cell morphology: (a) HPP/20%LMPP foams and (b) HPP/30%LMPP foams of five-fold expansion. Left: a cross-sectional image taken parallel to the core-back direction (thickness direction); Right: a cross-sectional image taken perpendicular to the core-back direction.

FIGURE S10. Surface roughness (*Sa*) of HPP foam with N_2 concentration of 0.11 % and 0.15 %.